

Received 7 December 2024, accepted 23 December 2024, date of publication 25 December 2024, date of current version 8 January 2025.

Digital Object Identifier 10.1109/ACCESS.2024.3523136



RESEARCH ARTICLE

Multifunctional Reconfigurable Millimeter-Wave Array Antenna

RAWAD W. ASFOUR[®], (Member, IEEE), SALAM K. KHAMAS[®], (Senior Member, IEEE), AND EDWARD A. BALL[®], (Senior Member, IEEE)

Communications Research Group, Department of Electronic and Electrical Engineering, The University of Sheffield, S1 3JD Sheffield, U.K.

Corresponding author: Rawad W. Asfour (rwsasfour1@sheffield.ac.uk)

This work was supported by The University of Sheffield Institutional Open Access Fund.

ABSTRACT This paper presents the design and implementation of an innovative 4-element multifunctional reconfigurability array antenna (MRAA) operating at 27.5 GHz, leveraging PIN diodes for enhanced functionality. By strategically controlling the alignment of PIN diodes, the antenna utilizes only two coplanar strip line biasing networks, streamlining its design and implementation. The proposed array demonstrates exceptional versatility by easily generating scanning beams at angles up to ±25° across three distinct polarizations: right-hand and left-hand circular polarizations and linear polarization. Furthermore, the system achieves a reconfigurable frequency interface between circular and linear polarizations, enhancing its adaptability to diverse communication scenarios. Through comprehensive analysis, the proposed MRAA exhibits commendable array gain, surpassing 10 dBic, and very good radiation efficiency exceeding 74%. This work marks the pioneering effort in designing a multifunctional reconfigurable array antenna for millimeter-wave (mmWave) applications. Additionally, the proposed array offers simplicity in design and outperforms existing counterparts operating at lower frequencies. A prototype has been fabricated, and measurement results demonstrate close agreement with simulation, validating the efficacy of the proposed design.

INDEX TERMS Circular polarization, loop antenna, millimeter wave, phased arrays, PIN diode, reconfigurable antennas.

I. INTRODUCTION

In light of the relentless pace at which technology advances within wireless communication systems, antennas, which stand as a fundamental component in contemporary wireless communications, are confronting ever-mounting demands to achieve heightened performance levels. This is imperative for effectively addressing intricate communication scenarios encompassing challenges like multipath interference and polarization mismatches. Consequently, the development of multifunctional and intelligent array antennas assumes paramount importance. Amid the various approaches employed to confront this challenge, reconfigurable antennas have emerged as a compelling solution due to their intrinsic flexibility and versatility.

The associate editor coordinating the review of this manuscript and approving it for publication was Tanweer Ali[®].

However, most reported studies on reconfigurable antennas have primarily focused on modifying a single antenna's parameter.

Moreover, despite the evident advantages of such antennas, they may prove inadequate in meeting the escalating requirements of high-speed communication systems, such as those used on the Internet of Things and 5G/6G applications. Consequently, over the past two decades, there has been an increased emphasis on proposing multifunctional reconfigurable antennas that can recompose more than one parameter.

The ability to furnish additional radiation modes offers considerable benefits, such as increased channel capacity through polarization reconfigurability and beam steering. On the other hand, a phased array's reconfigurable beam direction represents an economical and practical alternative to the high-cost phase shifters and RF chains commonly used for beam steering. An antenna array that offers



simultaneous polarization, frequency, and pattern reconfigurability addresses key challenges in modern communication systems.

One of the earliest demonstrations of the potential of multifunctional reconfigurable antenna (MRA) has been reported in [1], where a configuration of Radio Frequency Microelectromechanical Systems (MEMS) integrated antennas has been utilized in a multi-input multi-output (MIMO) system with several polarization states that have been achieved at 4.1 GHz and 6.4 GHz. Multifunctional reconfigurability has been attained using 64 square patches that are inter-connected to each other using 112 MEMS switches. Subsequently, a different study introduced a pattern and frequency reconfigurable annular-ring slot antenna, employing two small PIN diodes on the feeding microstrip line to connect/disconnect stubs for frequency tuning, and incorporating two larger PIN diodes on the annular ring slot to control radiation patterns at 5.2 GHz, 5.8 GHz, and 6.4 GHz [2]. In addition, textile circular patch antennas loaded by three varactor diodes to offer frequency, polarization, and pattern reconfigurability have been reported [3]. The first antenna switches between broadside and omnidirectional radiation modes over specific frequency ranges, while the second antenna switches the linear polarization between 0°, 120°, or 240° over a frequency range of 1.9-2.62 GHz. A frequency and pattern reconfigurable microstrip antenna has been designed using 6 varactor diodes to achieve a dual-band operation with a broadside pattern at 2.68 GHz and an omnidirectional pattern at 3.5 GHz [4]. In another study, a multifunctional microstrip antenna that offers three linear polarizations, and three main beam directions was demonstrated by utilizing 10 PIN diodes at 11 GHz [5].

Furthermore, a novel MRA was proposed using a parasitic substrate layer with 5×5 square metallic patches, known as pixels, incorporating 20 MEMS switches for the connection/disconnection of various pixels to achieve reconfigurability of frequency between 9 and 10 GHz with three radiation patterns [6]. However, it was highlighted that the pixeled planar surface requires many switches, which impacts the antenna efficiency and results in a complex fabrication process. Additionally, a multifunctional reconfigurable pixeled planar antenna was reported by utilizing 144 MEMS switches in a square matrix of 9×9 pixels, where frequency tuning has been demonstrated over a range of 4-7 GHz with reconfigurable radiation patterns and adjustable linear polarization at each frequency [7]. Moreover, a frequency and pattern reconfigurable pixeled monopole antenna was reported by utilizing 12 MEMS switches to alter the antenna geometry and achieve operating frequencies of 1.5 GHz, 3.5 GHz, 4.5 GHz, and 5.5 GHz with up to five radiation patterns at each frequency [8]. In a subsequent study, a frequency, pattern, and polarization reconfigurable antenna was reported by utilizing a single patch antenna in conjunction with a 6×6 parasitic pixel substrate that involved 60 PIN diodes to generate various combinations of pixels, albeit with a radiation efficiency range of 45%-55% [9]. Another MRAA has been reported using a four elements linear patch array, each loaded by a passive substrate of 4×4 pixels [10]. However, for simplicity, open circuits and hard-wired short circuits have been utilized instead of RF switches, providing radiation pattern and polarization reconfigurability in combination with a gain of 13.5 dBi. On the other hand, it is essential to note that pixel-based antennas involve complex biasing requirements for many switches placed above the antenna.

A different approach to designing MRAs using a liquid metal has been reported in [11], [12], [13], and [14]. For example, an MRA that offers pattern and linear polarization reconfigurability has been proposed using a dipole antenna over a frequency range of 1-2.2 GHz [11]. Furthermore, a bent monopole based on liquid metal has been proposed for frequency and polarization reconfigurability, where both left-hand circular polarization (LHCP) and right-hand circular polarization (RHCP) radiations have been achieved over a frequency band of 3-5 GHz [12]. Another liquid-metal-based antenna has been reported with frequency and polarization reconfigurability over a frequency range of 0.5-3.5 GHz [13]. Besides, frequency and polarization reconfigurability have also been achieved using a liquid metal over a frequency range of 2-8 GHz by switching a 3D-printed channel between the x and y linear polarization (LP) states [14]. Although a liquid-metal-based MRA offers continuous frequency tunability, a longer switching time is expected between various modes. Besides, the required mechanism to inject the liquid metal may be impractical at mmWave frequencies, considering the smaller physical dimensions of the antenna at such frequencies.

Another approach to design MRA using multiple ports has been proposed through varying the current distribution along a patch antenna by adjusting the phases of four feeding ports to achieve pattern and polarization reconfigurability over a frequency range of 4-5 GHz [15]. LHCP and RHCP radiation have been achieved over a main beam scanning range of $\pm 70^{\circ}$. Both single-element and 4×4 element arrays have been considered. However, using multiple ports increases power consumption, size, complexity and requires numerous wire connections. This represents a considerable challenge to adapt at mmWave frequencies, owing to the limited physical space to accommodate several SMAs with sufficient de-coupling between them. Furthermore, multifunction digitally controlled reconfigurable antennas have recently been reported in combinations with multi-port feeding, and PIN diodes [16], [17].

This review of existing literature reveals a notable absence of MRAA designed for mmWave applications since all the reported designs are focused on antennas operating at lower frequencies with mainly modest radiation efficiencies and complex structures that may be impractical at mmWave frequencies. It should be noted that a mmWave multifunctional array has been reported in [18] in which only the polarization is reconfigurable as the beam-steering was achieved using a beamformer board. Therefore, this article is focused on



the design, fabrication, and measurements of such an antenna. Building upon the mmWave phased array and reconfigurable single antenna designs introduced in [19] and [20] to achieve a multifunctional reconfigurable mmWave array, which has not been reported earlier. The reconfigurable single loop antenna introduced in [20] will be used as an element from which a multifunctional reconfigurable array is designed to provide polarization, pattern, and frequency reconfigurability by utilizing PIN diode switches in a simple structure that offers high efficiency.

A. CONTRIBUTIONS

In addressing the challenges, this study presents the following contributions:

1) DESIGN AND FABRICATION OF A COST-EFFECTIVE MULTIFUNCTIONAL RECONFIGURABLE ARRAY ANTENNA

A low-profile, cost-effective 4-element reconfigurable phased array system is designed and fabricated, specifically operating at 27.5 GHz. Within each array element, two strategically designed gaps accommodate PIN diodes, serving as switches. These diodes enable the selection of the desired polarization by toggling between forward-bias and reverse-bias states, enhancing the adaptability of the antenna system. In addition, the one-input-four-output feeding network incorporates four transmission line phase shifters, with each section introducing a distinct phase shift. The degree of phase shift is contingent upon the bias applied to the PIN diodes and the length of the corresponding transmission line segment. This innovative approach enhances beam control and array performance.

2) UTILIZATION OF ONLY TWO DC BIASING NETWORKS

Coplanar strip lines (CPS), including photonic band gap (PBG) elements, have been utilized for the DC biasing; one to switch the polarization of the four elements and another to control the main beam direction. Incorporating only two networks to bias 16 PIN diodes represents considerable simplicity and eliminates further efficiency deterioration owing to the absence of lumped RF chokes or capacitors. Consequently, the proposed antenna system achieves higher efficiency, providing a more robust and effective solution.

3) IMPROVED PERFORMANCE

In addition to the mmWave operation and higher radiation efficiency, the proposed MRAA offers favourable radiation characteristics such as high gain, broader impedance, and axial ratio (AR) bandwidths that outperform most of those reported in earlier studies.

These contributions collectively address challenges in designing efficient mmWave antennas with multifunctional reconfigurability, offering a comprehensive and innovative framework for developing advanced phased array systems for 5G and B5G communication systems.

The paper's organization unfolds as follows: Section II introduces the configuration and design principles of the mmWave MRAA and the relevant parameters. Following this, Section III outlines the utilization of electrical switching at mmWave frequencies and the operating mechanism, illustrating the integration of PIN diodes within the proposed array. Section IV provides comprehensive details concerning the prototypes, simulations, fabrication processes, and measurements of the proposed reconfigurable array antenna at 27.5 GHz. Section V presents a performance comparison between the proposed configuration and reported counterparts. Finally, Section VI delivers a summary and concluding remarks for the paper.

II. MRAA CONFIGURATION

A. CONSTITUENT LAYERS OF THE PROPOSED RECONFIGURABLE ARRAY

Fig. 1 illustrates the proposed configuration in which five layers are utilized including the array elements and feed network as the first layer. The second layer comprises Rogers RT/Duroid RO4003C substrate material, featuring a dielectric constant of 3.55 and a loss tangent ($tan\delta$) of 0.0027, with a thickness of 0.508 mm. Several distinct advantages drive the choice of Rogers substrate, such as low dielectric constant, high efficiency, and ease of manufacturability. Another dielectric substrate employed in this design is the FR-4, characterized by respective dielectric constant and thickness of 4.3 and 0.5 mm. This layer primarily functions as an insulator, facilitating the interface between the ground plane layer and the bottom layer, which includes the CPS-PBG biasing networks. The Rogers and FR-4 substrate layers encapsulate a central copper ground plane with a thickness of 0.07 mm. Each substrate possesses dimensions of 37 mm in width and 40 mm in length. A lower auxiliary copper ground plane, measuring 40 mm in width and 8.5 mm in length, is utilized. This supplementary ground plane assumes a critical role in grounding, particularly when securing the connector in place. The multi-layer structure is essential to provide the required isolation between the DC biasing network and the antenna array. Otherwise, the performance of the phased array will be severely impacted by any interference with the biasing network.

B. ARRAY AND FEED NETWORK

'Fig. 2 depicts the configuration of a 1×4 reconfigurable linear antenna array designed to operate at 27.5 GHz, featuring an inter-element spacing of 4.65 mm, approximately equivalent to 0.5λ 0 at the operating frequency. Each constituent element within the array exhibits an identical design, characterized by two concentric loops, with the outer loop as the active element. The outer loop for each array element incorporates two gaps that house the PIN diodes, functioning as switches capable of toggling forward-bias and reverse-bias states to select the desired polarization senses. The optimization of the outer loop's gaps, $\Delta \varphi_1 = \Delta \varphi_2$, plays a pivotal role



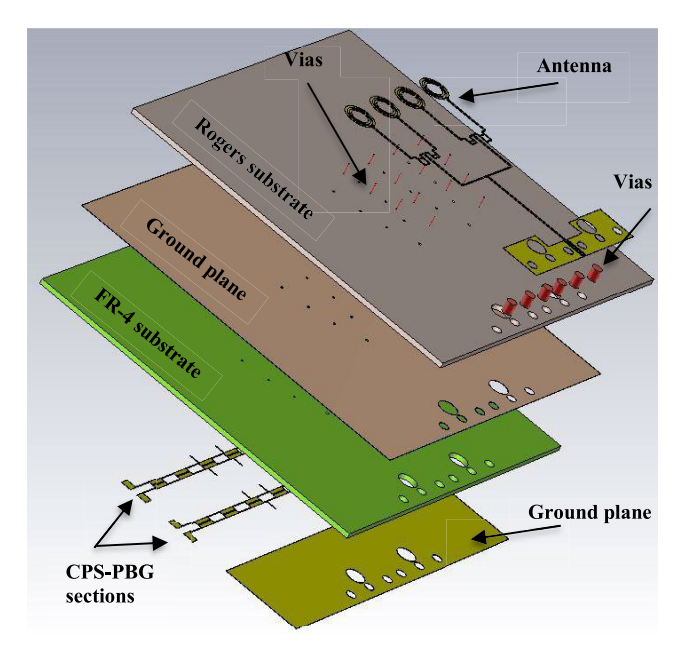


FIGURE 1. The layers of the proposed reconfigurable array.

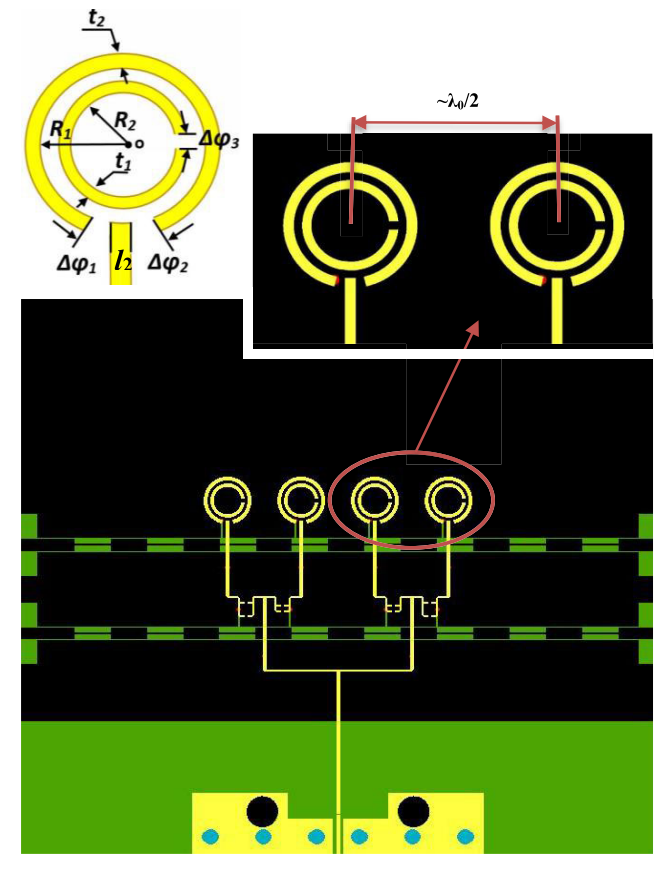


FIGURE 2. The geometry of the proposed reconfigurable array and the DC biasing networks.

in establishing a travelling wave current distribution along the loop. This distribution is indispensable for the generation of diverse circular polarization states. In addition, a smaller gap $\Delta \varphi_3$ within the inner loop has been selected to enhance the CP bandwidth. Furthermore, selecting the loop antenna's radius

TABLE 1. Parameters of the proposed array configuration.

Symbol	Quantity	Value
R_I	outer loop radius	1.27mm
R_2	parasitic loop radius	0.875 mm
t_I	outer loop width	0.26 mm
t_2	parasitic loop width	0.21 mm
Pad_l	pads length	8.9 mm
Pad_w	pads width	3.96 mm
l_2	transmission line width	0.25 mm
l_3	the gap between the transmission line & pads	0.2 mm
a_0	antenna thickness	0.035 mm
h	The thickness of the substrate	0.508 mm
t	reflector thickness	0.07 mm
Sub_x	substrate length	37 mm
Sub_v	substrate width	40 mm
$\Delta \phi_1$	outer loop gap 1	$20^{\rm o}$
$\Delta \phi_2$	outer loop gap 1	20°
$\Delta \phi_3$	inner loop gap	18°

is critical to ensuring that the circumference approximates one effective wavelength, denoted as λ_{eff} . The inter-element spacing of the antenna array is judiciously chosen to maximize gain and minimize side lobe levels (SLL). The feeding of the antenna arrays is facilitated by a parallel feed network employing microstrip transmission lines with widths of 0.2 mm and 0.25 mm. The configuration parameters for the reconfigurable array are summarized in Table 1.

Fig. 3(a) introduces a one-input-four-output feeding network, which integrates four transmission line phase shifters. Each section introduces a distinct phase shift within this network, as depicted in Figs. 3(b) and 3(c). This phase shift is contingent upon the specific bias applied to the PIN diode and the length of the corresponding transmission line segment. This method harnesses transmission lines to achieve the requisite phase shift, constituting what is recognized as a true-time surface current distribution of the proposed array with CPS bias line only at 27.5 GHz delay [21]. This approach is particularly advantageous in phased arrays with parallel feeding, as it enhances the system's bandwidth. True-time delay is especially well-suited for broad-spectrum applications, as it maintains the stability of the primary beam direction across a spectrum of frequencies.

True-time delay encompasses integrating delay sections along the transmission lines within the feed network. These delay sections align with the precise phase shifts needed. Adjusting the time delay for each element makes it possible to manage the aggregate phase shift across the array, enabling accurate beam steering control. The required microstrip line physical length, l, to generate a phase shift (delay) of $\Delta\Phi$ between adjacent elements can be calculated as:

$$\Delta \Phi = k_e l = \sqrt{\varepsilon_e} k_0 l, \tag{1}$$

where k_0 is the free space wavenumber, is the effective dielectric constant that can be calculated as. We can calculate the physical length by establishing the main beam angle θ as a function of the phase shift between adjacent elements,



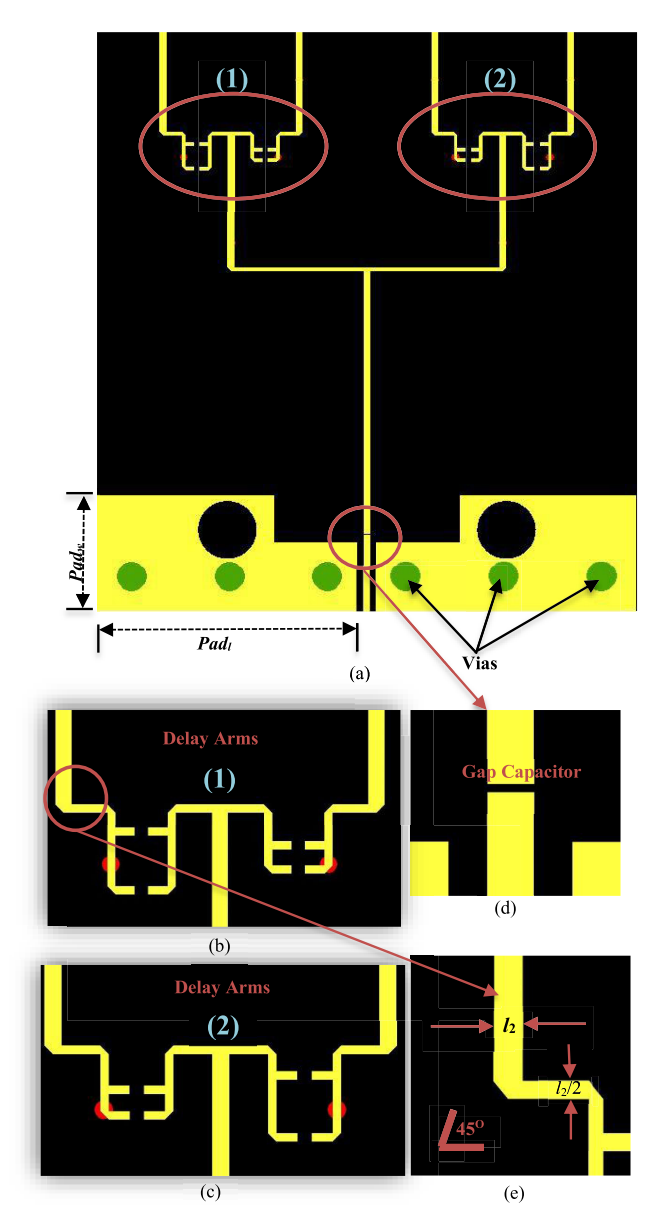


FIGURE 3. (a) Corporate feed network, (b) left-hand phase shifters, (c) right-hand phase shifters, (d) gap capacitor, (e) chamfered corners.

denoted as $\Delta\Phi$ [18]. For example, if the same lengths of feeding lines are used, then a broadside gain is achieved with a higher gain compared to a steered beam owing to the impact of the single element's radiation pattern.

A design enhancement is introduced to enhance matching and elevate the array's performance, featuring the implementation of 45° chamfered corners on the transmission lines, as depicted in Fig, 3(e). These measures ensure that the utilized corporate feed supports a focused main beam in the required direction. Additionally, Fig. 3(d) highlights the presence of a gap capacitor, designed through microstrip line patterning, providing a modest capacitance of approximately 0.1 pF. This component prevents DC from traversing to the network analyzer. The gap distance of 0.05 mm was selected, ensuring that the desired capacitance of 0.1 pF is

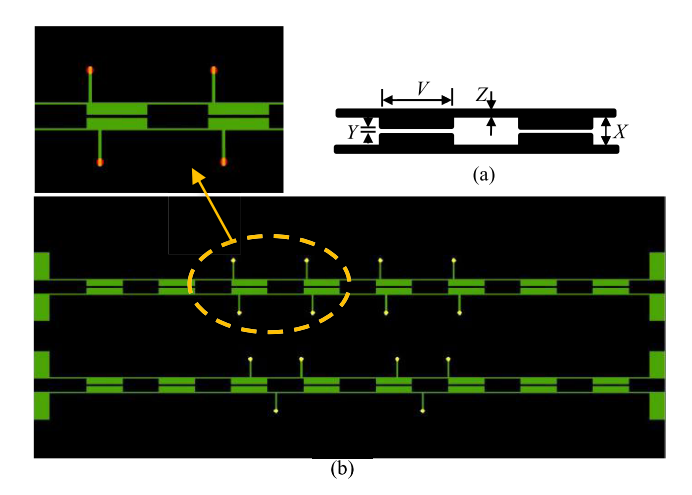


FIGURE 4. (a) Structure of CPS bias line and PBG, (b) Top CPS-PBG connected to outer loops and bottom CPS-PBG connected to phase shifters.

achieved given the specified feedline dimensions and material properties [21]. Integrating vias into the design yields several benefits, encompassing improved grounding, mitigation of surface waves, and bandwidth expansion. Each possesses a radius of 1 mm and is situated at 4 mm intervals, center to center.

C. DC BIASING NETWORKS

It should be noted that the existence of antennas, feeding, and biasing networks on the same substrate surface represents a challenging task and complications that can be avoided by moving the biasing network to another substrate, FR4 in this case, which is positioned at the other side of the shared ground plane surface. However, the connections of the biasing networks to the diodes have been implemented by utilizing metalized vias. Such an arrangement provides optimum isolation between the biasing network and the antenna.

A coplanar strip line is connected to the antenna element through vias that connect the CPS and an array to provision DC bias. The current distribution along the bias line leads to undesirable RF current leakage into the antenna, turning the bias line into an unintended antenna system component. Consequently, the antenna's key characteristics, including resonance frequency, input impedance, and radiation pattern, are affected. To mitigate this issue, developing a novel bias line structure is imperative, one that effectively carries the requisite DC bias current while preventing the unwanted flow of RF current.

To curtail RF current propagation. within the coplanar strip line, a PBG structure featuring a $0.25\lambda_{\rm eff}$ periodicity is deployed. Fig. 4(a) illustrates this PBG structure, which comprises a series of high and low quarter-wavelength transformer sections. The gap width between the high-impedance section CPS line is X, the PBG cell length is V, is Y, and the width of the CPS line is Z. Due to the relatively small size of the CPS line, especially in the mmWave frequencies designs,



TABLE 2. Parameters for the CPS- PBG structure.

Symbol	Value (mm)		
$\overline{}$	2.2		
X	0.7		
Y	0.1		
Z	0.1		
$Pad_{x} \ Pad_{y}$	1.8		
Pad_{v}	1		

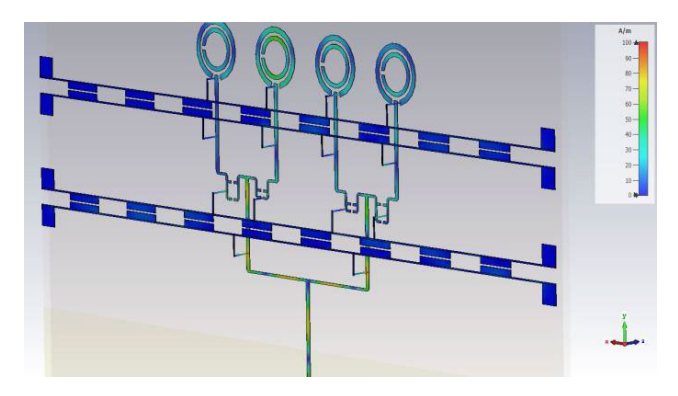


FIGURE 5. Surface current distribution of the proposed antenna with CPS-structure at 27.5 GHz.

two solder pads have been employed, as shown in Fig. 4(b). The design parameters for the CPS bias line and PBG are summarized in Table 2. Fig. 5 presents the surface current distribution of the antenna with a PBG bias line at 27.5 GHz. It is evident that the PBG bias line effectively cuts off the RF current from flowing to the second PBG cell, preventing the undesired current leakage.

In the proposed design, the alignment of the PIN diodes on the loop antennas has been chosen so that all the diodes can be ON or OFF simultaneously. Hence a single biasing network is sufficient for the 8 PIN didoes. The same applies to the other 8 PIN diodes placed on the feed network to control the main beam direction. Therefore, only two biasing networks have been utilized for the whole configuration, which results in cost savings, lower losses, and a simplified design structure. In addition, fourteen vias have been thoughtfully incorporated to establish connections between the CPS and the PIN diodes placed on the array configuration. This strategy stems from the unique approach in positioning the PIN diodes within the outer loop gaps,

necessitating using two vias for each loop. As a result, eight vias are dedicated to precisely controlling polarization senses. In addition, the placement strategy of the PIN diodes on the phase shifters minimizes the vias count as well, with only six vias serving the purpose of beam steering within a only six vias serving the purpose of beam steering within a range of \pm 25°.

Within the proposed array operating at 27.5 GHz, the MA4AGFCP910 PIN diode is employed [22], which has been utilized in several studies as a switch at millimetre wave

TABLE 3. Switch configuration for desired operation moods (1 = on, 0 = off) for the main beam direction of.

Mode	1	2	3	4	5	6
	LHCP	LHCP	RHCP	RHCP	LP	LP
θ_0	-25°	+25°	-25°	+25°	-25°	+25°
\mathbf{D}_1	1	1	0	0	0	0
D_2	0	0	1	1	0	0
D_3	1	1	0	0	0	0
D_4	0	0	1	1	0	0
D_5	1	1	0	0	0	0
D_6	0	0	1	1	0	0
D_7	1	1	0	0	0	0
D_8	0	0	1	1	0	0
D_9	0	1	0	1	0	1
D_{10}	1	0	1	0	1	0
\mathbf{D}_{11}	0	1	0	1	0	1
D_{12}	1	0	1	0	1	0
D_{13}	1	0	1	0	1	0
D_{14}	0	1	0	1	0	1
D_{15}	1	0	1	0	1	0
D ₁₆	0	1	0	1	0	1

frequencies [23], [24], [25], [26], [27]. Notably, accurate modelling of these PIN diodes has been conducted utilizing lumped elements within the equivalent RLC circuits of both forward-biased and reverse-biased diodes. The corresponding RLC equivalent circuit parameters are as follows: Total capacitance (C_T) = 0.018 pF, total inductance (L_T) = 1 nH, parallel resistance (R_L) = 15 K Ω , and series resistance (R_S) = 5.2 Ω .

III. SWITCHING MECHANISM AT MMWAVE FREQUENCIES

Fig. 6 illustrates the integration of PIN diodes within the proposed array, where each of the sixteen PIN diode switches is numbered to designate their respective states across various operational modes. Comprehensive details regarding the switch configurations and their corresponding operational modes are presented in Table 3. When a DC is applied to the CPS lines, the strategically positioned vias facilitate the current's path reaching the PIN diodes, enabling the application of forward and reverse bias as required. Six distinct operating modes are achieved. Each is associated with different polarization, and beam steering direction based on the status of the PIN diodes. Notably, the states of the PIN diodes, specifically from D_1 to D_8 , positioned on each outer loop of the array, are meticulously controlled to effect changes in the polarization. Meanwhile, the PIN diodes fixed on the transmission lines, specifically D₉ to D₁₆, are leveraged to enable precise beam steering within a range of $\pm 25^{\circ}$. It should be noted that a wider beam steering is achievable, albeit with a narrower CP bandwidth.

To steer the beam towards an angle of $+25^{\circ}$, the following PIN diodes are engaged in the ON state: D_9 , D_{11} ,

 D_{14} , and D_{16} , while simultaneously switching D_{10} , D_{12} , D_{13} , and D_{16} to the OFF state. Conversely, a complementary configuration redirects the beam towards an angle



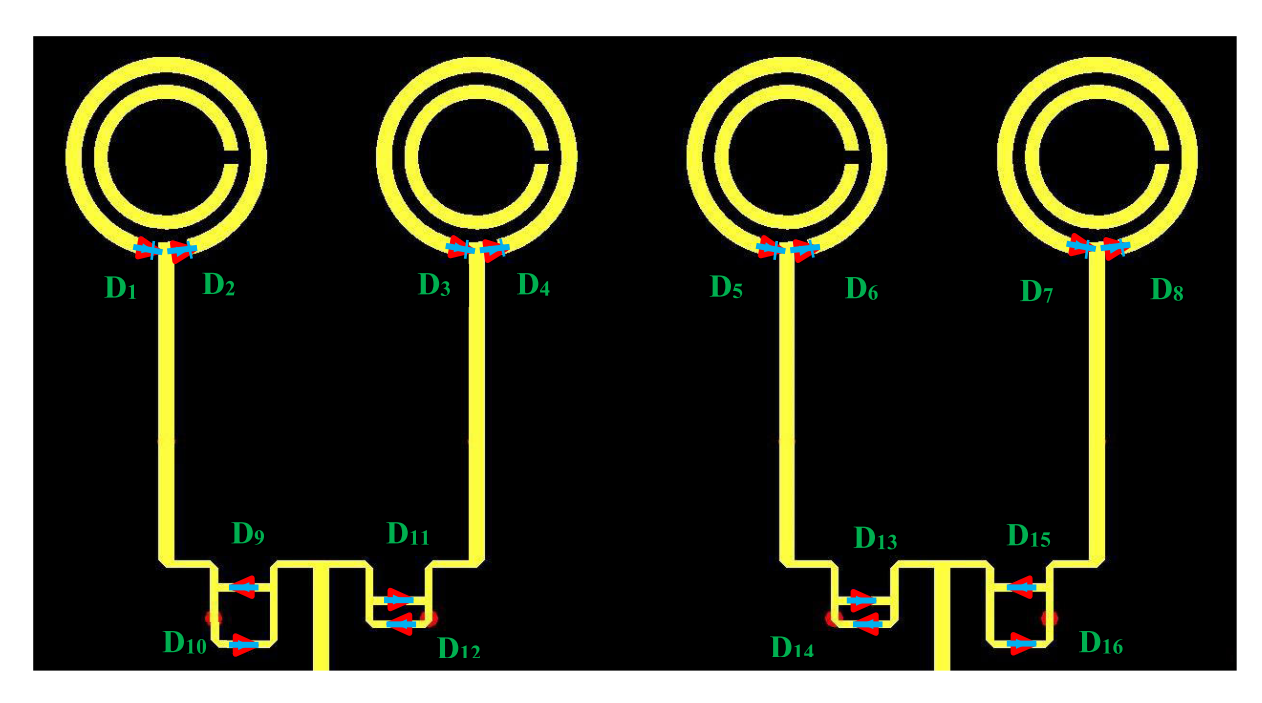


FIGURE 6. The incorporation of 16 PIN diodes into the proposed array that results in an MRAA.

of -25° . This entails biasing D_{10} , D_{12} , D_{13} , and D_{16} in the forward state, while D_9 , D_{11} , D_{14} , and D_{16} are subjected to a reverse bias. This level of control enables the array to achieve precise beam steering in multiple directions, enhancing its versatility and adaptability.

Three cases are attainable in the context of polarization: LHCP, RHCP, and LP. LHCP configuration is realized by placing D_1 , D_3 , D_5 , and D_7 in forward bias states while concurrently holding D_2 , D_4 , D_6 , and D_8 in reverse bias. Conversely, the PIN diode cases are inverted to achieve RHCP, with D_2 , D_4 , D_6 , and D_8 in forward bias and D_1 , D_3 , D_5 , and D_7 in reverse bias. Lastly, for LP, PIN diodes D_1 to D_8 are set to a zero-bias, or unbiased, state, effectively holding them in a neutral position and allowing the antenna to operate without imparting circular polarization. This precise control over polarization cases empowers the array able requirements. In addition, LP radiation is achieved at a different resonance frequency of 26 GHz, which results in mmWave MRAA with adjustable polarization, main beam direction, and frequency.

IV. FABRICATION AND MEASUREMENTS

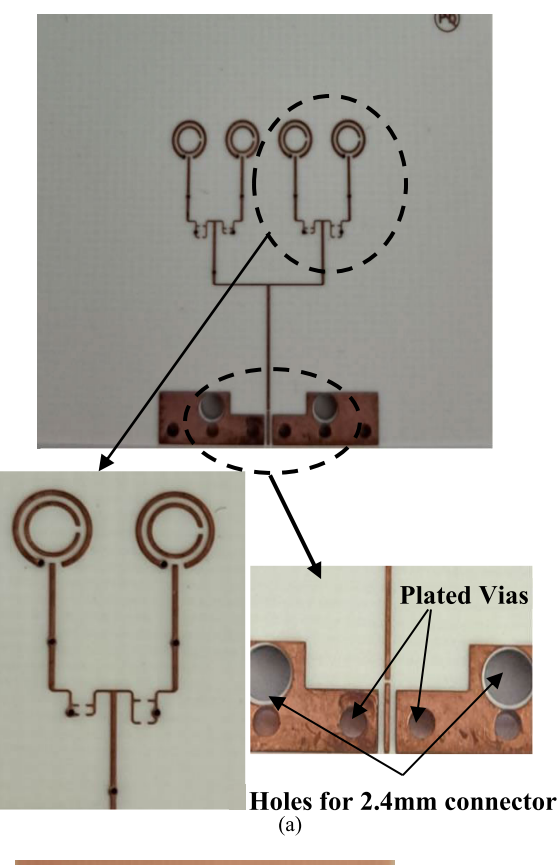
This section showcases the fabrication and measurement results. Precisely, one prototype of the suggested MRAA is fabricated and tested to verify the design. The measurements have been conducted using the E5071C mmWave vector network analyzer (VNA) and the National mmWave Measurement Facility (NmmMF) [28]. The reflection coefficient was measured using a 2.4 mm SMA connector and an N5245B VNA. Fig. 7 presents photographs of the fabricated reconfigurable array antenna by Wrekin [29], and Fig. 8 illustrates the connection between the proposed antenna and the

DC power supply. Measurements were conducted to verify the simulations, focusing on return losses and axial ratio at beam steering angles of -25° and $+25^{\circ}$ and considering three different polarization types: LHCP, RHCP, and LP.

The comparisons of these results are illustrated in Figs. 9 and 10, revealing close agreement between simulations and measurements. Additionally, the findings highlight consistently good impedance matching across all main beam directions. In the first scenario, the simulation indicates that configuring the antenna to operate in the LHCP case results in percentage impedance bandwidths of approximately 9.96% and 9.1% for the evaluated beam steering angles $(-25^{\circ} \text{ and } +25^{\circ})$, respectively. The corresponding measured results show bandwidths of around 6.8% and 6.75%. In the second scenario, when RHCP cases are considered for the same beam steering angles, the simulated antenna array exhibits percentage impedance bandwidths of approximately 8.6% and 8.4%. In comparison, the measured results show around 5.9% and 5.7%, respectively. Furthermore, the results indicate that LHCP and RHCP cases demonstrate nearly symmetrical performance, a desirable characteristic for specific applications. Differences between measurement and simulations can be attributed to the assembly of the PIN diodes using silver paint and experimental errors. Overall, these findings underscore the reliability of the simulations, highlight the effectiveness of impedance matching, and suggest potential applications for LHCP and RHCP cases.

In Fig. 10, the achieved reflection coefficient in the LP case is depicted under the scenario where the PIN diodes of the loops, D_1 - D_8 , are under zero bias, and the beam steering angles are the same, i.e. -25° and $+25^{\circ}$. Notably, the figure reveals successful matching over a narrow band centred





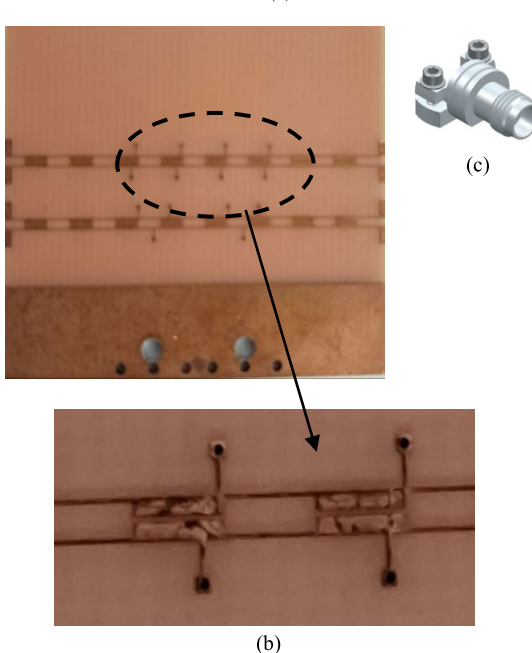
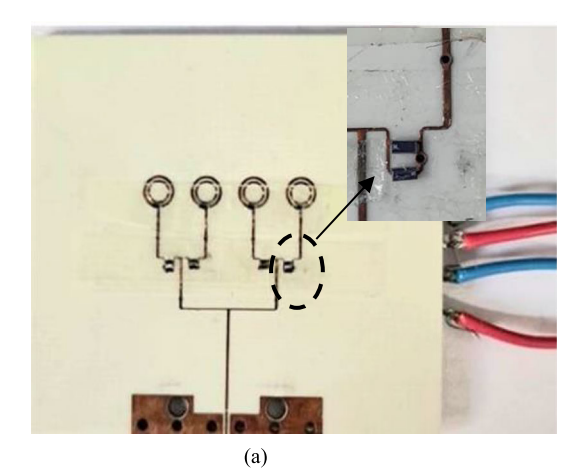


FIGURE 7. Fabricated MRAA prototype (a) Top view, (b) Bottom view, (c) 2.4 mm SMA connector.

at 26 GHz, with considerably narrower bandwidths than those in the CP cases. Specifically, the simulation demonstrates bandwidths of 3.28% and 3.5%, while the measurements show slightly narrow bandwidths at 2.46% and 2.42%. These findings suggest that in addition to achieving reconfigurable polarization and beam steering, the antenna also possesses



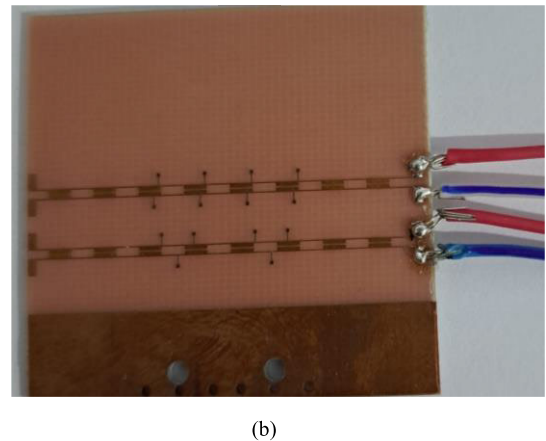


FIGURE 8. MRAA prototype with wires for DC connections (a) Top view, (b) Bottom view.

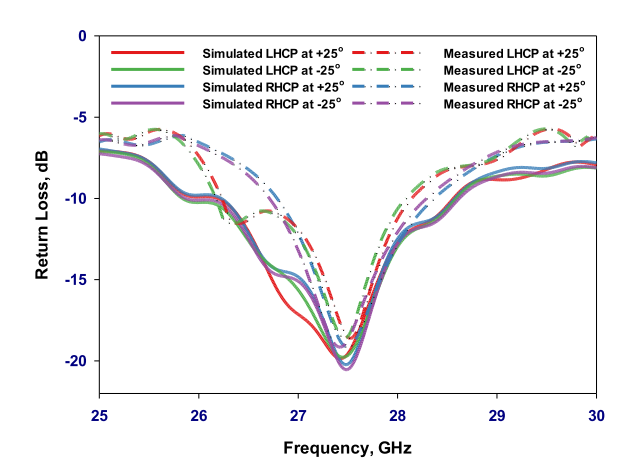


FIGURE 9. Return losses as a function of frequency across various CP senses and beam directions.

reconfigurable frequency capabilities when utilizing linear polarization. Therefore, the proposed antenna introduces a multifunctional reconfiguration as it enables tuning frequency, polarization, and radiation patterns using 16 PIN diodes and two biasing networks, offering a versatile solution for various applications.



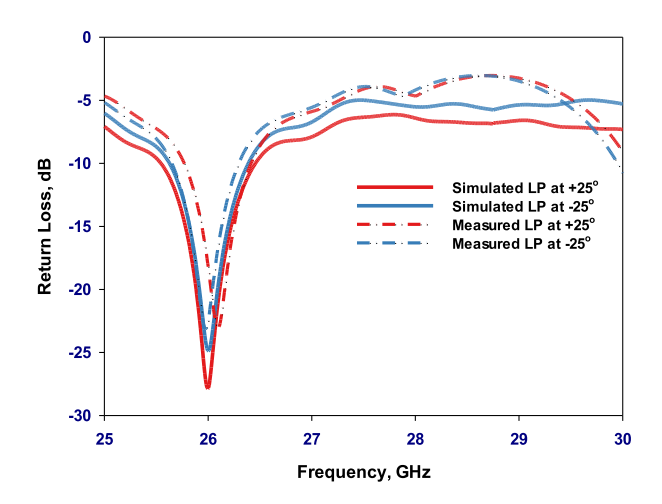


FIGURE 10. Return losses of the mmWave reconfigurable array antenna operating in the LP case at different main beam directions.

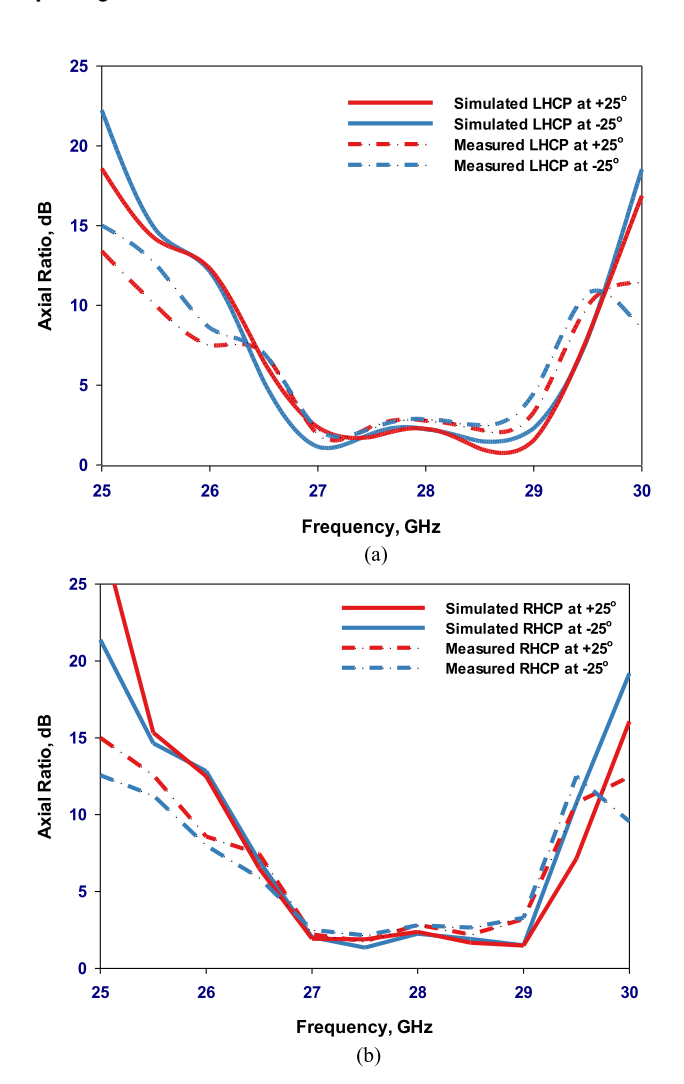
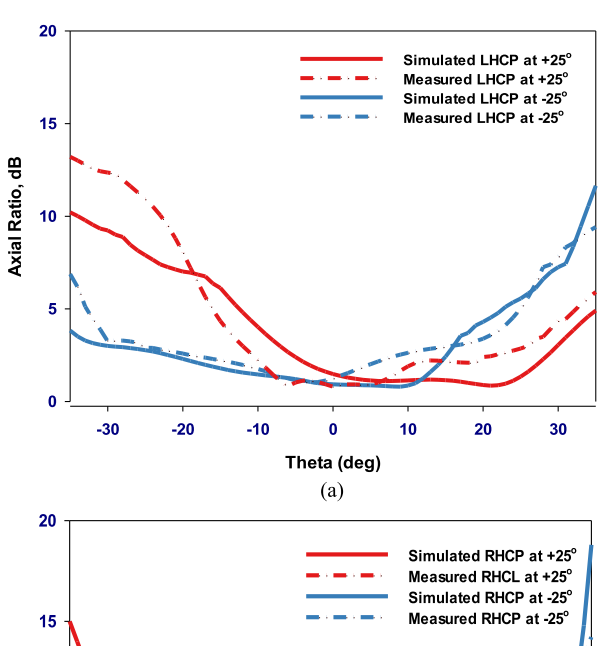


FIGURE 11. Axial ratio for circular polarization senses and beam steering angles in the main beam direction (a) LHCP (b) RHCP.

Fig. 11(a) and 11(b) showcase the measured and simulated axial ratios for LHCP and RHCP cases at beam steering



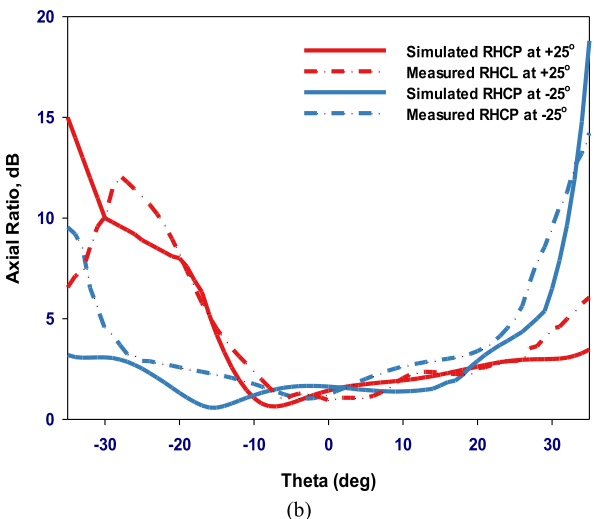


FIGURE 12. AR as a function of polar angle θ at 27.5 GHz for two polarization senses: (a) LHCP and (b) RHCP.

angles of -25° and $+25^{\circ}$. In the LHCP scenario, the simulated 3 dB axial ratio bandwidths cover 8.7% and 8.1% within beam steering angles of -25° and $+25^{\circ}$, respectively. The measured 3 dB AR bandwidth in the same LHCP scenario registers around 6.1% and 6.3%, demonstrating close agreement with simulations. Conversely, the simulated 3 dB AR bandwidths in the RHCP scenario are roughly 8.2% and 8.5% within beam steering angles of -25° and $+25^{\circ}$, respectively. Correspondingly, the measured outcomes show bandwidths of approximately 6.2% and 6.1%, centred at 27.5 GHz; furthermore, Fig. 12(a) and 12(b) illuminate the 3 dB axial ratio beamwidth for the LHCP and RHCP configurations at beam steering angles of -25° and $+25^{\circ}$, showcasing a commendable convergence between measured results and simulations at the pivotal frequency of 27.5 GHz. In the LHCP scenario, when the main beam is directed at -25° , the experiment yielded a measured AR beamwidth spanning from $(-26^{\circ} \text{ to } 14^{\circ})$, harmonizing closely with the simulated range of $(-28^{\circ} \text{ to } 15^{\circ})$. Similarly, with the main beam steered to +25°, the measured AR beamwidth extended from

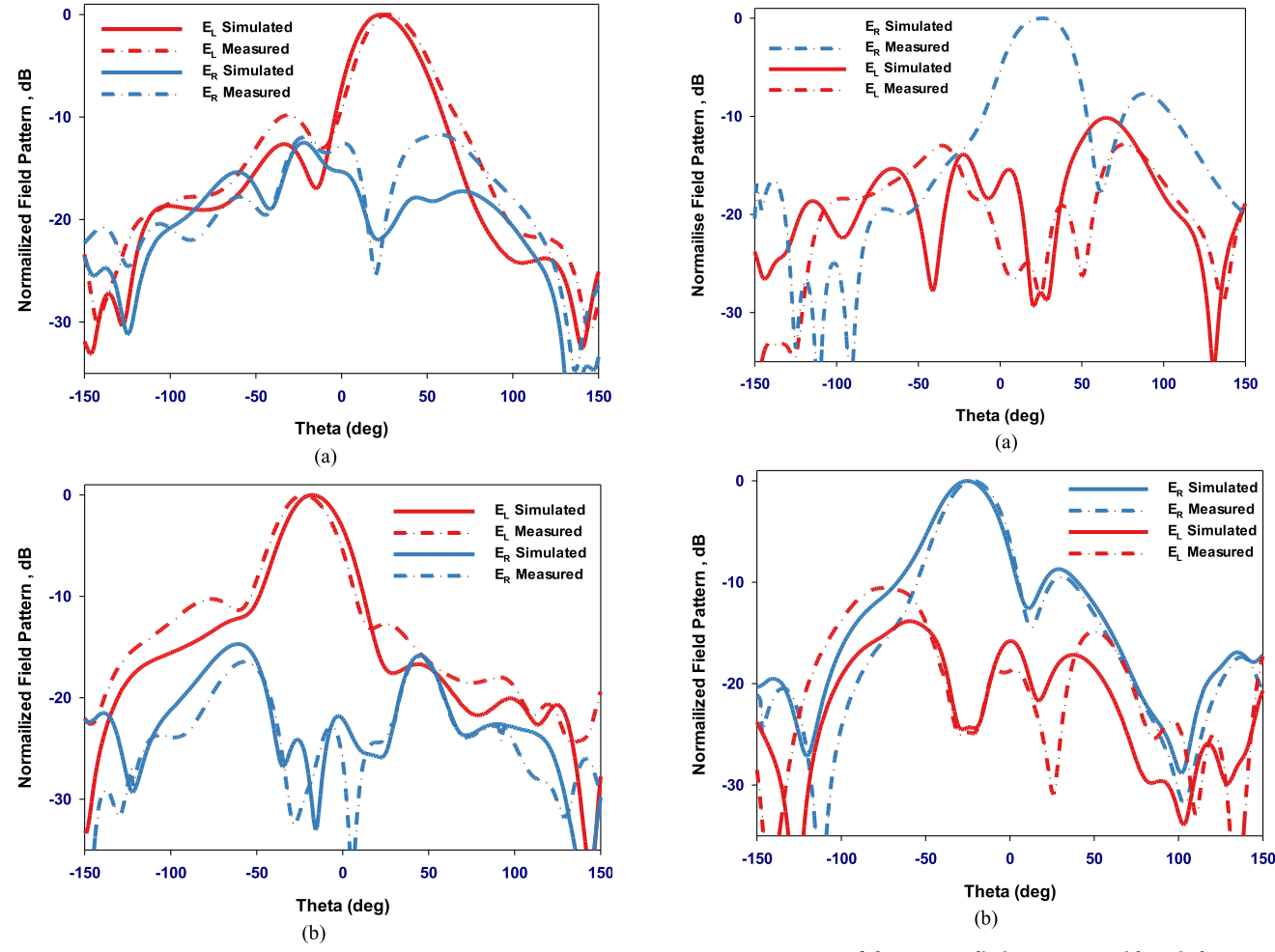


FIGURE 13. ER of the LHCP radiation patterns with main beam directions of (a) $+25^{\circ}$ and (b) -25° .

FIGURE 14. EL & ER of the RHCP radiation patterns with main beam directions of (a) $+25^{\circ}$ and (b) -25° .

 $(-12^{\circ} \text{ to } 26^{\circ})$, aligning seamlessly with the simulated range of $(-7^{\circ} \text{ to } 29^{\circ})$. Switching to the RHCP scenario, when the main beam is at -25° , the measured AR beamwidth unfolded from $(-26^{\circ} \text{ to } 15^{\circ})$, aligning effectively with the simulated range of $(-30^{\circ} \text{ to } 18^{\circ})$. Finally, with the main beam pointed at $+25^{\circ}$, the measured AR beamwidth spanned from $(-11^{\circ} \text{ to } 26^{\circ})$, in accord with the simulated range of $(-13^{\circ} \text{ to } 27^{\circ})$. This alignment between experimental findings and simulations attests to our methodology's precision and underscores this research's substantive contribution.

Fig. 13 and Fig. 14 illustrate the normalized simulated and measured radiation patterns of the E_L and E_R components at the $\phi=0^\circ$ principal plane, corresponding to LHCP and RHCP cases achieved by the reconfigurable array with two beam steering angles (-25° and $+25^\circ$). The results reveal a substantial alignment between experimental and simulated data, albeit with minor discrepancies attributed to measurement errors in the mmWave frequency range. In some cases, E_L is stronger than E_R by more than 20 dB in the main beam direction, corresponding to an LHCP sense. Conversely, when the E_R component exceeds the strength of E_L ,

it signifies an RHCP. However, the difference between $E_L\&E_R$ is reduced as the elevation angle is shifted from $\pm 25^\circ$, which indicates the degradation of the circular polarization level. By controlling all cases of the PIN diodes, different main beam polarization and steering can be switched.

Fig. 15 presents the normalized radiation patterns at 26 GHz in the antenna's E-plane when the PIN diodes on the loop antennas are under zero bias with close agreement between simulated and measured results. This configuration enables the radiation of LP wave at varying operating frequencies and two distinct beam steering angles of +25° and -25° . The proposed array has successfully achieved six cases, incorporating reconfigurable frequency, polarization, and beam steering functionalities. Fig. 16 illustrates the maximum realized gains for both circular polarization and linear polarization modes across all cases as the main beam is steered to angles of -25° and $+25^{\circ}$. Additionally, the findings highlight an increase in side-lobe levels attributed to the beam steering effect. From these results, it can be observed that for Cases 1 to 4, which correspond to CP radiation, the simulated realized gain is circa 10.3 dBic



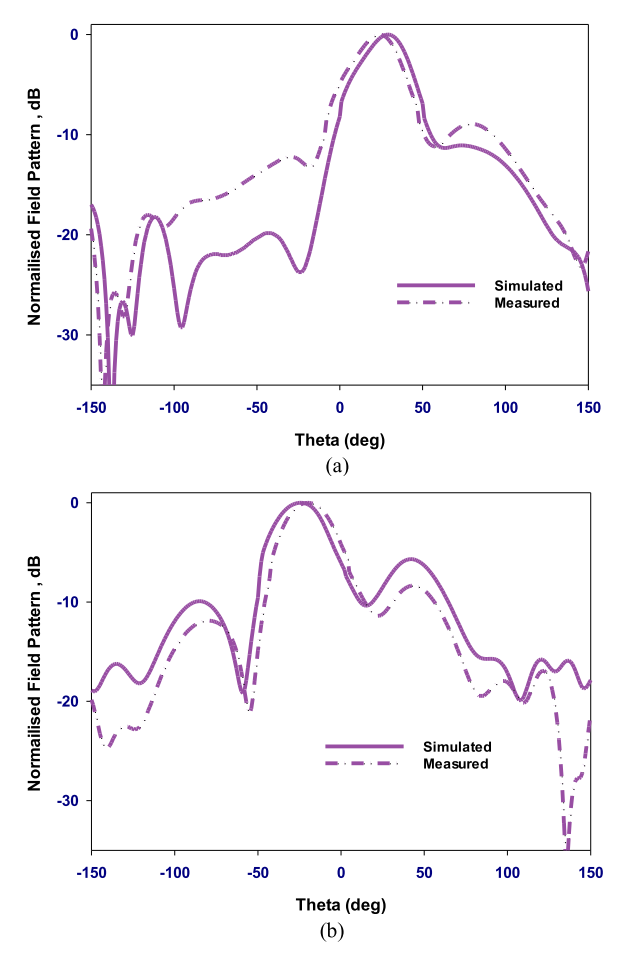


FIGURE 15. Normalized radiation patterns with main beam directions of (a) $+25^{\circ}$ and (b) -25° .

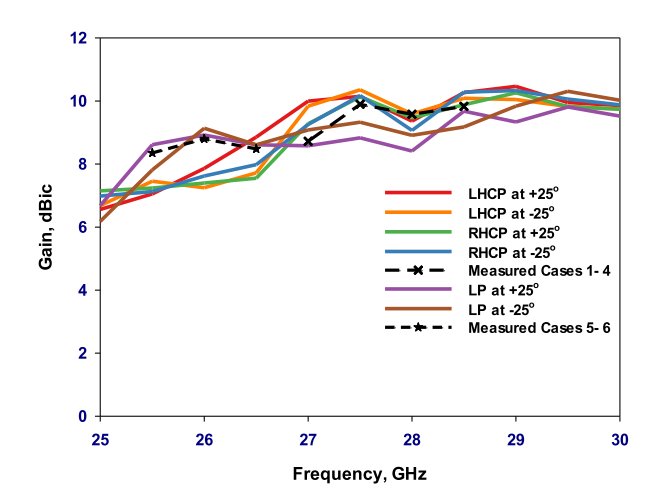


FIGURE 16. Realized gains for different polarizations and different main beam directions of the mmWave MRAA.

at 27.5 GHz, while in Cases 5 and 6, which correspond to LP case, the antenna exhibits a slightly lower realized gain of approximately 9.1 dBi at 26 GHz. This agrees with the measurements, which can be explained by the different loading

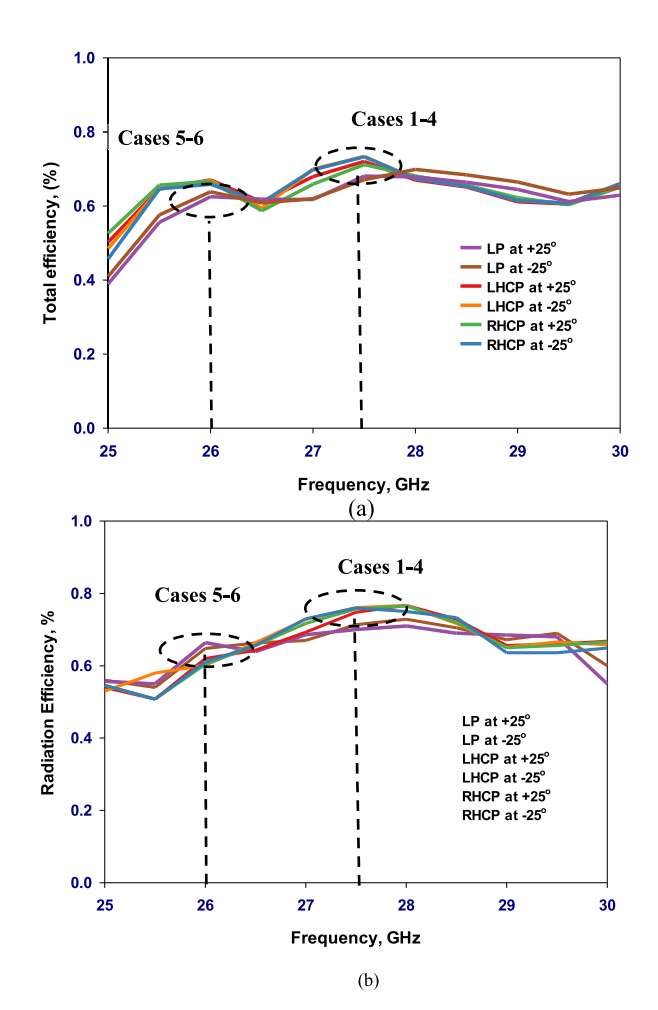


FIGURE 17. Efficiency for different polarizations of the proposed mmWave MRAA is (A) total efficiency and (b) radiation efficiency.

impedances offered to the antenna by biased diodes in cases 1-4 and unbiased diodes in cases 5-6, which could alter the current distribution and reduce the efficiency. Significantly, the simulated total and radiation efficiency remain consistently high across various scenarios. It reaches approximately 73% and 76% for cases 1 to 4 while 64% and 67% for cases 5 to 6, aligning with the desired bandwidth, as illustrated in Fig. 17. The lower efficiency in the LP case could be attributed to the higher resistance offered by the unbiased PIN diodes. This finding emphasizes the remarkable performance of the multifunctional reconfigurable antenna within the mmWave frequency range.

Figure 18 provides an example demonstrating the stable operation of the antenna at two distinct frequencies 26.5 GHz and 28.5 GHz. The results show good agreement between simulation and measurement for the RHCP component, with the main beam being steered to an angle of approximately -25° .

V. PERFORMANCE COMPARISON

A comprehensive comparison between the performance of the proposed antenna and existing literature is presented

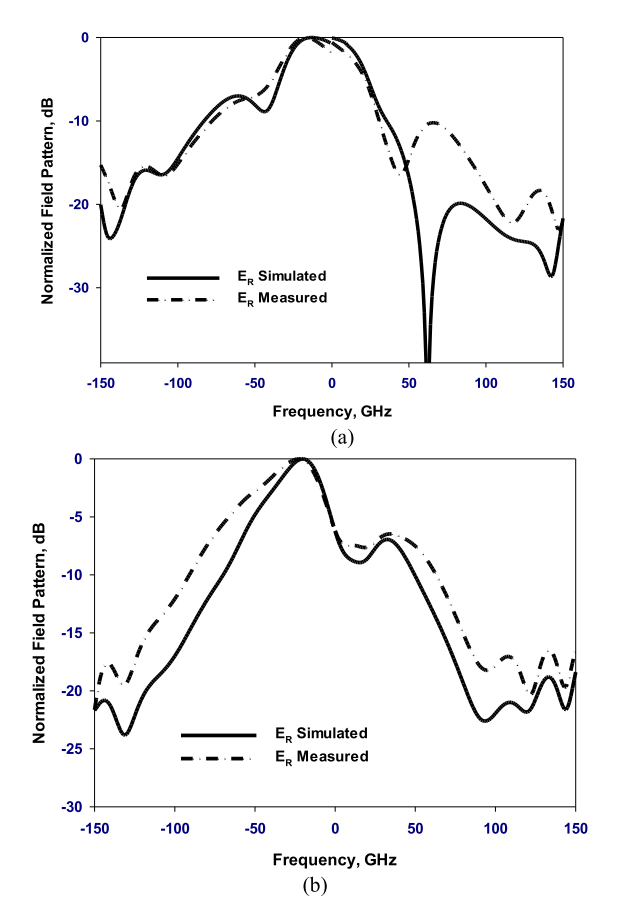


FIGURE 18. Demonstration of stable antenna operation with main beam steering to \sim -25 $^{\circ}$ (RHCP) at (a) 26.5 GHz and (b) 28.5 GHz.



FIGURE 19. Measurement setup inside the anechoic chamber.

in Table 4, underscoring the uniqueness and significance of the findings in this study. Notably, the comparison is primarily drawn with antennas operating at lower frequencies, up to 11 GHz, as no array with multifunctional reconfigurability has been reported in the literature that operates at higher frequencies, thus highlighting the novelty of the presented research.

Table 4 reveals that only two reported configurations of MRAA offer reconfigurability across the three

TABLE 4. Comparison of the proposed antenna performance against reported mraa prototypes.

[1] Ref.	Freq. GHz 4.1, 6.4 5.2,	Antenna & Switching Mechanism MIMO,	BW S ₁₁		Gain dBi	η %	Reconfigur ability of
[1]	6.4	MIMO,					
[1]	6.4	,		AR			
	5.2	112 MEMS	3	_ _	_	_	Polarization Frequency
	6.4	Slot, 4 PIN diodes		NA		80	Pattern Frequency
[3]	1.4-2.8 2.0-2.5 1.9-2.6	PA, 3 Varactors		NA	-0.7 6.5 3.8	42 95 65	Frequency Pattern Polarization
	2.7, 3.5	PA, 6 Varactors	_	NA	7.5 5	94 76	Frequency Pattern
[5]	11	PA, 10 MEMS		NA	8, 7.2, 7.4	1	Pattern Polarization
[9]	10	Pixel, 20 MEMS	5	NA		1	Frequency Pattern
[7]	4.5, 7	81 PA, 144 MEMS	1.5- 4	NA	3. 4.7	46	Pattern Frequency Polarization
[8]	2.5	PA-Pixel, 12 MEMS	16	NA	6	70	Frequency Pattern
[6]	2.7	PA-Pixel, 60 PIN Diodes	2.8	_	4	50	Pattern Frequency Polarization
[10]	5.4-5.6	4 PAs-Pixel, 24*	3	1.8	13.5	1	Pattern Polarization
[11]	0.8-3	Crossed dipole, Liquid Metal	_	-	0.3 -1.7	41 - 70	Frequency Polarization
[12]	1.5	Dipole, Liquid Metal	_	NA	2.1	95	Pattern Polarization
[13]	3-5	Monopole, Liquid Metal	40	37. 5 48. 8	2.2		Frequency Polarization
[14]	2-7	Microstrip, Liquid Metal	5.9	_	5.9	90	Frequency Polarization
[15]	4-5	PA, Array, Multi-port	22	_	_	75	Pattern Polarization
	1.3- 2.2	PA, Array, 4 port, Digital, 4 PIN diodes	2	NA	15.5	54 - 59	Frequency Polarization
[17]	2.5	1×4 DRs, 32 PIN Diodes, Digital	12.5	2.4	9	60	Pattern Polarization
This work	28	1×4 Loops, 16 PIN Diodes	9	8	10	73	Pattern Frequency Polarization

* Hard wired, PA: Patch Antenna

key parameters—frequency, radiation pattern, and polarization [7], [9], albeit with a higher number of operating modes compared to the current study. However, the proposed design, employing only 16 PIN diode switches, stands out significantly against counterparts utilizing 144 MEMS and 60 PIN diodes in [7] and [9], respectively. This valuable reduction in component count is complemented by superior features such as mmWave operation, increased gain, high efficiency, and broader bandwidths.



Moreover, existing designs face challenges in adapting to mmWave frequencies due to complexities arising from excessive switch counts and/or parasitic substrates [1], [6], [7], [9], [10], or the utilization of metal liquids [11], [12], [13], [14], multiple ports [15], [16], and DR elements associated with assembly and bonding complexities [17]. Additionally, CP radiation is predominantly reported in studies, often with unspecified or narrower AR bandwidths [1], [9], [10], [11], [14] and [17]. However, wider CP bandwidths have been noted in [13], [15], and [17], albeit with design limitations. Furthermore, the proposed design exhibits exceptional gain

* Hard wired, PA: Patch Antenna and radiation efficiency, ranking among the highest in Table 4. It represents a pioneering effort to showcase the potential of a multifunctional reconfigurability for millimeter-wave frequencies, making it particularly suitable for 5G/B5G and 6G systems. Additionally, the design offers distinct advantages including simplicity and enhanced bandwidth, gain, and efficiency performance.

VI. CONCLUSION

This study has introduced a novel MRAA design tailored for mmWave frequency applications, with a focus on achieving multifunctional reconfigurability and designing an efficient biasing network for 16 PIN diodes. Notably, the implementation required only two biasing networks, a significant reduction compared to existing literature. The fabrication and measurement of a prototype demonstrated a close alignment between measured and simulated results. These findings underscore the potential of the proposed MRAA in facilitating reconfigurability for critical antenna parameters such as pattern, polarization, and frequency. Moreover, the incorporation of additional diodes enables the attainment of desired main beam steering directions. Furthermore, the scalability of the design, with the addition of more array elements or modifying the array geometry, promises enhanced gain and a broader scanning range, further solidifying the versatility and efficacy of the proposed approach. These performance improvements require the utilization of efficient optimization algorithms in the design of a millimeter wave multifunctional reconfigurable array.

ACKNOWLEDGMENT

The authors wish to thank the UKRI National mmWave Measurement Facility for performing measurements for this work.

REFERENCES

- [1] B. A. Cetiner, H. Jafarkhani, J.-Y. Qian, H. J. Yoo, A. Grau, and F. De Flaviis, "Multifunctional reconfigurable MEMS integrated antennas for adaptive MIMO systems," *IEEE Commun. Mag.*, vol. 42, no. 12, pp. 62–70, Dec. 2004, doi: 10.1109/MCOM.2004.1367557.
- [2] S. Nikolaou, R. Bairavasubramanian, C. Lugo, I. Carrasquillo, D. C. Thompson, G. E. Ponchak, J. Papapolymerou, and M. M. Tentzeris, "Pattern and frequency reconfigurable annular slot antenna using PIN diodes," *IEEE Trans. Antennas Propag.*, vol. 54, no. 2, pp. 439–448, Feb. 2006, doi: 10.1109/TAP.2005.863398.

- [3] Q. H. Dang, S. J. Chen, N. Nguyen-Trong, and C. Fumeaux, "Multifunctional reconfigurable wearable textile antennas using coplanar reconfiguration modules," *IEEE Trans. Antennas Propag.*, vol. 71, no. 5, pp. 3806–3815, May 2023, doi: 10.1109/TAP.2023.3242459.
- [4] N. Nguyen-Trong, L. Hall, and C. Fumeaux, "A frequency- and pattern-reconfigurable center-shorted microstrip antenna," *IEEE Antennas Wireless Propag. Lett.*, vol. 15, pp. 1955–1958, 2016, doi: 10.1109/LAWP.2016.2544943.
- [5] P.-Y. Qin, S.-L. Chen, and Y. J. Guo, "A compound reconfigurable microstrip antenna with agile polarizations and steerable beams," in *Proc. Int. Symp. Antennas Propag. (ISAP)*, Phuket, Thailand, Oct. 2017, pp. 1–2, doi: 10.1109/ISANP.2017.8228879.
- [6] D. Rodrigo, Y. Damgaci, M. Unlu, B. A. Cetiner, J. Romeu, and L. Jofre, "Antenna reconfigurability based on a novel parasitic pixel layer," in *Proc. 5th Eur. Conf. Antennas Propag. (EUCAP)*, Rome, Italy, Apr. 2011, pp. 3497–3500.
- [7] A. Grau Besoli and F. De Flaviis, "A multifunctional reconfigurable pixeled antenna using MEMS technology on printed circuit board," *IEEE Trans. Antennas Propag.*, vol. 59, no. 12, pp. 4413–4424, Dec. 2011, doi: 10.1109/TAP.2011.2165470.
- [8] D. Rodrigo and L. Jofre, "Frequency and radiation pattern reconfigurability of a multi-size pixel antenna," *IEEE Trans. Antennas Propag.*, vol. 60, no. 5, pp. 2219–2225, May 2012, doi: 10.1109/TAP.2012.2189739.
- [9] D. Rodrigo, B. A. Cetiner, and L. Jofre, "Frequency, radiation pattern and polarization reconfigurable antenna using a parasitic pixel layer," *IEEE Trans. Antennas Propag.*, vol. 62, no. 6, pp. 3422–3427, Jun. 2014, doi: 10.1109/TAP.2014.2314464.
- [10] Z. Li, D. Rodrigo, L. Jofre, and B. A. Cetiner, "A new class of antenna array with a reconfigurable element factor," *IEEE Trans. Antennas Propag.*, vol. 61, no. 4, pp. 1947–1955, Apr. 2013, doi: 10.1109/TAP.2012.2234073.
- [11] M. Wang, M. R. Khan, M. D. Dickey, and J. J. Adams, "A compound frequency- and polarization-reconfigurable crossed dipole using multidirectional spreading of liquid metal," *IEEE Antennas Wireless Propag. Lett.*, vol. 16, pp. 79–82, 2017, doi: 10.1109/LAWP.2016.2556983.
- [12] G. B. Zhang, R. C. Gough, M. R. Moorefield, K. J. Cho, A. T. Ohta, and W. A. Shiroma, "A liquid-metal polarization-pattern-reconfigurable dipole antenna," *IEEE Antennas Wireless Propag. Lett.*, vol. 17, pp. 50–53, 2018, doi: 10.1109/LAWP.2017.2773076.
- [13] X. H. Wang, H. W. Pan, L. Z. Wang, X. W. Shi, and Y. Xu, "A simple frequency- and polarization-reconfigurable bent monopole antenna based on liquid metal," *IEEE Antennas Wireless Propag. Lett.*, vol. 22, pp. 950–954, 2023, doi: 10.1109/LAWP.2022.3225213.
- [14] V. T. Bharambe, J. Ma, M. D. Dickey, and J. J. Adams, "Planar, multifunctional 3D printed antennas using liquid metal parasitics," *IEEE Access*, vol. 7, pp. 134245–134255, 2019, doi: 10.1109/ACCESS.2019.2942058.
- [15] G. Yang, Q. Cheng, J. Li, S. Zhang, S. Gao, and X. Chen, "A multifunctional array system based on adjustable-phase antenna for wireless communications," *IEEE Trans. Antennas Propag.*, vol. 71, no. 5, pp. 4552–4557, May 2023, doi: 10.1109/TAP.2023.3243987.
- [16] J. Wu, X. Lu, W. Wang, J. Han, G. Xu, and Z. Huang, "Design of a compact polarization-agile and frequency-tailored array antenna with digital-controllable radiation beams," *IEEE Trans. Antennas Propag.*, vol. 70, no. 2, pp. 813–822, Feb. 2022, doi: 10.1109/TAP.2021.3111325.
- [17] Z. Wang and Y. Dong, "Phase and polarization digitally modulated array using reconfigurable DR element: Proposal, design, and verification," *IEEE Trans. Antennas Propag.*, vol. 71, no. 5, pp. 4102–4114, May 2023.
- [18] G. Mishra and S. K. Sharma, "A multifunctional full-polarization reconfigurable 28 GHz staggered butterfly 1-D-beam steering antenna," *IEEE Trans. Antennas Propag.*, vol. 69, no. 10, pp. 6468–6479, Oct. 2021, doi: 10.1109/TAP.2021.3070226.
- [19] R. W. Asfour, S. K. Khamas, and E. A. Ball, "Design and measurements of circularly polarized millimeter-wave phased array antenna using time delay transmission lines," *IEEE Access*, vol. 11, pp. 122016–122028, 2023, doi: 10.1109/ACCESS.2023.3329088.
- [20] R. Asfour, S. K. Khamas, and E. A. Ball, "Cost-effective design of polarization and bandwidth reconfigurable millimeter-wave loop antenna," vol. 23, no. 24, 2023, Art. no. 9628, doi: 10.3390/s23249628.
- [21] T. C. Edwards and M. B. Steer, Foundations for Microstrip Circuit Design. Chichester, U.K.: Wiley, 2016.
- [22] MA4AGP907 MA4AGFCP910—Mouser Electronics. Accessed: Oct. 19, 2023. [Online]. Available: https://www.mouser.com/datasheet/ 2/249/MA4AGP907_FCP910-838114.pdf



- [23] Md. A. Towfiq, I. Bahceci, S. Blanch, J. Romeu, L. Jofre, and B. A. Cetiner, "A reconfigurable antenna with beam steering and beamwidth variability for wireless communications," *IEEE Trans. Antennas Propag.*, vol. 66, no. 10, pp. 5052–5063, Oct. 2018, doi: 10.1109/TAP.2018.2855668.
- [24] J. Zhang, S. Zhang, Z. Ying, A. S. Morris, and G. F. Pedersen, "Radiation-pattern reconfigurable phased array with p-i-n diodes controlled for 5G mobile terminals," *IEEE Trans. Microw. Theory Techn.*, vol. 68, no. 3, pp. 1103–1117, Mar. 2020, doi: 10.1109/TMTT.2019.2949790.
- [25] K. Trzebiatowski, M. Rzymowski, L. Kulas, and K. Nyka, "Simple 60 GHz switched beam antenna for 5G millimeter-wave applications," *IEEE Antennas Wireless Propag. Lett.*, vol. 20, pp. 38–42, 2021, doi: 10.1109/LAWP.2020.3038260.
- [26] J. Romeu, S. Blanch, L. Pradell, A. Barlabé, J.-M. Rius, M. Albert-Gali, L. Jofre-Roca, C. Mazzucco, and R. Flamini, "Lens based switched beam antenna for a 5G smart repeater," *IEEE Antennas Wireless Propag. Lett.*, vol. 22, no. 10, pp. 2482–2486, Oct. 2023.
- [27] W. Fu, Y. Cai, P. Mei, G. Frølund Pedersen, and S. Zhang, "Electronically reconfigurable filtering reflectarray antenna using polarization conversion elements with controllable conversion zeros," *IEEE Trans. Antennas Propag.*, vol. 72, no. 9, pp. 7359–7364, Sep. 2024, doi: 10.1109/TAP.2024.3433577.
- [28] UKRI National Millimeter Wave Facility. Accessed: Oct. 3, 2023. [Online]. Available: https://www.sheffield.ac.uk/mm-wave/
- [29] Wrekin Circuits Ltd. Accessed: Oct. 3, 2023. [Online]. Available: https://www.wrekin-circuits.co.uk/



RAWAD W. ASFOUR (Member, IEEE) was born in Ajdabiya, Libya, in 1983. He received the Master of Science degree in mobile and satellite communication from the University of South Wales, U.K., in 2017, and the Ph.D. degree in electrical and electronic engineering from The University of Sheffield, U.K., in 2024. He was a Teaching Associate with the Department of Electronic and Electrical Engineering, The University of Sheffield, from March 2024 to October 2024.

Since October 2024, he has been a Senior Research Officer with the University of Essex, Colchester, U.K. His research interests include full-duplex radio systems, reconfigurable millimeter-wave antennas, and phased array antennas. He received the Award of Excellence during the bachelor's degree.



SALAM K. KHAMAS (Senior Member, IEEE) received the B.Sc. degree in electronic engineering from the University of Technology, Baghdad, Iraq, in 1985, and the Ph.D. degree from The University of Sheffield, Sheffield, U.K., in 1992. From 1993 to 1998, he was a Research Associate with the Electronic and Electrical Engineering Department, The University of Sheffield. From 1998 to 2002, he was a Software Engineer with Alcatel Telecommunications and then in Nor-

tel Networks. Since 2002, he has been an Academic Staff with the Electronic and Electrical Engineering Department, The University of Sheffield. His research interests include millimeter wave antennas, dielectric resonator antennas, antenna arrays, and computational electromagnetics.



EDWARD A. BALL (Senior Member, IEEE) was born in Blackpool, U.K., in November 1973. He received the Master of Engineering degree (Hons.) in electronic systems engineering from the University of York, York, U.K., in 1996. After graduating, he worked in industry for 20 years, first spending 15 years working as an Engineer, a Senior RF Engineer, and finally the Principal RF Engineer with Cambridge Consultants Ltd., Cambridge, U.K. Then, he spent five years as

the Principal RF Engineer and a Radio Systems Architect with Tunstall Healthcare Ltd., Whitley, U.K. In November 2015, he joined the Department of Electronic and Electrical Engineering, The University of Sheffield, Sheffield, U.K., where he is currently a Reader in RF engineering. His research interests include radio technology from RF system design, RF circuit design (sub-GHz to mm-wave), and the application of radio technology to real-world industrial and commercial problems. He has a particular passion for RF hardware design. He is a member of IET and is a Chartered Engineer.

• • •